Acta Scientiarum
http://periodicos.uem.br/ojs
ISSN on-line: 1807-8664
Doi: 10.4025/actascitechnol.v43i1.50488

Effect of autogenous GTAW on the reciprocating sliding wear behavior of a carbon martensitic steel

Thalita Cristina De Paula*, Cintia Cristiane Petry Mazzaferro, Daniela Fátima Giarollo, Gelsa Edith Navarro Hidalgo and Breno Basso

Universidade Federal do Rio Grande do Sul, Av. Paulo Gama, 110, 90130-120, Porto Alegre, Rio Grande do Sul, Brazil. *Author for correspondence. E-mail: tdepaula@outlook.com

ABSTRACT. Martensitic steels have been successfully employed in resource-based industries where components must endure aggressive conditions. In industrial practice, many parts of these components are joined by welding techniques. The aim of this work was to understand the influence of welding on the wear resistance of quenched and tempered carbon martensitic steel subjected to dry linear reciprocating sliding micro-wear tests. Weld-joints were produced using autogenous Gas Tungsten Arc Welding process (GTAW). Micro-wear tests were performed at base metal (BM), weld metal (WM), coarse grained heat affected zone (CG-HAZ) and lowest hardness region of heat affected zone (LHR-HAZ). LHR-HAZ was softened during welding process so plastic deformation was facilitated, and consequently adhesion, material displacement and micro-ploughing. WM and CG-HAZ presented a similar martensitic structure, which explain the similarities found on wear behavior. These regions presented the lowest worn volume average values (*w*). It was interesting to note that despite its highest microhardness value, the highest *w* was observed for BM. For some BM samples, debris had a key role promoting material loss by micro-cutting which causes great extent of material removal compared to other micro-wear mechanisms as micro-ploughing and adhesion. Due to debris action BM also presented a great dispersion in *w* results. The results suggest that material loss of welded joint and BM was strongly controlled by micro-wear mechanisms.

Keywords: micro-wear; ball-on-flat; abrasion; martensite; HAZ-softening.

Received on October 21, 2019.
Accepted on July 15, 2020.

Introduction

The usage of martensitic steels in resourced-based industries can be effective for minimizing costs due to wear, thus extending the service life (Mindivan, 2013). The fine grains of their martensitic structure create characteristics features of high strength, toughness, and resistance to abrasive wear (Białobrzeska, Dziurka, Żak, & Bała, 2018; Białobrzeska & Kostencki, 2015; Frydman, Konat, & Pękalski 2008; Mendez et al., 2014). These properties are obtained through a specific combination of thermomechanical processes and a strictly selected chemical composition that includes low quantities of phosphorus and sulphur (Białobrzeska & Kostencki, 2015). Mishra et al. (2019), highlighted that the addition of low quantities of boron in martensitic steels promotes grain refinement, thus improving strength levels and toughness. In order to improve the wear resistance, these martensitic low-alloyed steels are generally tempered to modify the balance between mechanical properties, and in particular to improve toughness and ductility while keeping a relatively high hardness (Xu, Zwaag, & Xu, 2016).

A significant amount of studies on wear resistance of martensitic steels were also developed (Białobrzeska & Kostencki, 2015; Hacısalihoğlu, Yildiz, & Çelik, 2018; Hernandez, Hardell, Winkelmann, Ripoll, & Prakash, 2015; Mindivan, 2013; Pawlak, Białobrzeska, & Konat, 2016;). Białobrzeska and Kostencki (2015) investigated the abrasive wear characteristics of selected low alloy boron steels in both field experiments and laboratory tests. The obtained results showed that hardness had a secondary role in controlling the wear rate. Results also indicated that abrasive wear rate depends strongly on the predominant mechanism of wear, which in turn is dependent on the microstructure. The authors highlighted that in their study, micro-cutting was the predominant micro-wear mechanism in material removal.

Welding techniques are widely used in industrial practice. The quality of welded joints mainly depends on mechanical properties of the weld zone and HAZ, which in turn is influenced by chemical composition and metallurgical variations of the weld zone. In other words, the quality of welded joints depends on welding process (Pujari, Patil, & Mewundi, 2018). Gas Tungsten Arc Welding (GTAW) and Gas Metal Arc Welding (GMAW) are the most used welding processes. However, GMAW offers problems such as melt and distortion, especially for thin workpieces (Pujari, Patil, & Mewundi, 2018). The welded joint between thin plates are typically made by GTAW. One of its main advantages is its relatively shallow penetration achievable during autogenous welding (Vasantharaja, Vasudevan, & Parameswaran, 2019).

The welding heat input may cause degradation of the favorable mechanical properties of these steels by changing their microstructure, these changes are particularly likely to affect the morphology and size of the martensite or bainite needles (Białobrzeska & Kostencki, 2015) resulting in hardness drops. This phenomenon is known as heat affected zone softening (HAZ softening). Past researches have shown that HAZ softening on welded joints of martensitic steels was observed mostly in the inter-critical and sub-critical heat affected zone (respectively IC-HAZ and SC-HAZ) (Biro, McDermid, Vignier, & Zhou, 2014; Hokkirigawa & Kato, 1988; Krishnan, Toppo, Basak, & Ray, 2006; Lu, Peer, Abke, Kimchi, & Zhang, 2018; Pandey, Mahapatra, Kumar, Daniel, & Adhithan, 2019; Pouranvari, Sobhani, & Goodarzi, 2018; Wang, Yang, Sun, Liu, & Li, 2016).

Despite its significance in wear behavior, the effect of weld resulting microstructure and HAZ softening has not received adequate attention. In this study, worn volume and micro-wear mechanisms were evaluated in the weld metal (WM), coarse grained heat affected zone (CG-HAZ), lowest hardness region of the heat affected zone (LHR-HAZ) and base metal (BM) of a wear-resistant steel welded joint. This work aims to analyze the influence of weld resulting microstructure on the wear resistance of a selected martensitic steel subjected to a reciprocating sliding micro-wear test.

Experimental details

The chemical composition of the base material used in this study and its carbon equivalent (CE) according to International Institute of Welding (IIW) is presented in Table 1 and Equation 1, respectively. Its microstructure is fully composed by small grains of tempered martensite as showed in Figure 1. CE formula is used to estimate the weldability of steels; it determines if preheat or post-welding heat treatments are necessary. For the selected martensitic steel used in this work preheat and post-welding treatments was not necessary (SSAB, 2019).

Table 1. Chemical composition of the selected martensitic steel.

Elements (max wt%)	C	Si	Mn	P	S	Cr	Ni	Mo	B	Fe	CE_{IIW}
BM	0.184	0.215	1.187	0.018	0.015	0.037	0.035	0.001	0.003	Bal.	0.389

$$CE_{IIW} = \frac{Mn}{6} + \frac{Cr+Mo+V}{5} + \frac{Cu+Ni}{15} \quad (1)$$

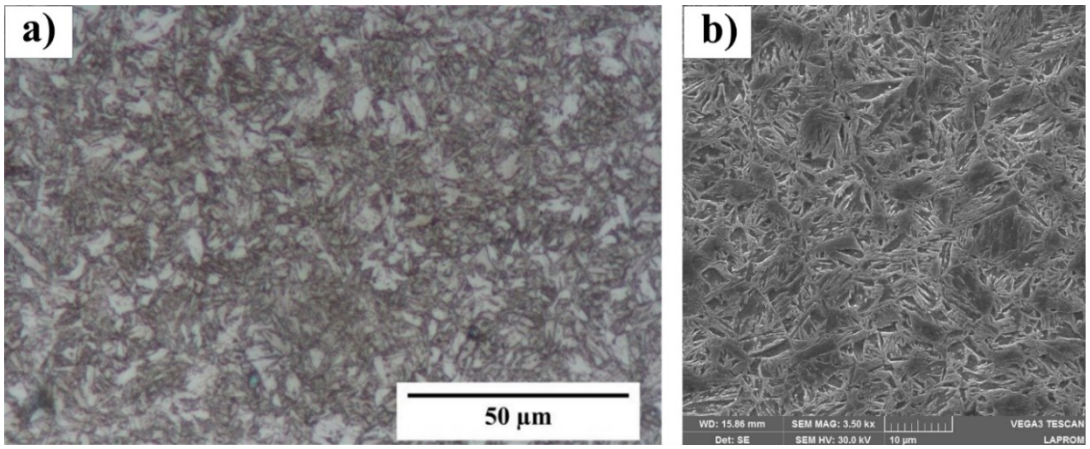

Figure 1. Typical microstructure of the base metal steel in the received condition obtained by: a) optic microscopy (OM); and b) scanning electron microscopy (SEM).

The weld-joint was produced by single pass butt-welding of 1 mm thick samples of approximately 300 x 100 mm, using a MA1400 Yaskawa welding robot and a Trans Plus Synergic 4000R power source. The joints were produced using autogenous GTAW, which is a high-quality joint process employed in thin workpieces where the usage of filler metal is not required. The welding parameters used in this work and the corresponding welding energy (E) are listed in Table 2. E can be determined by Equation 2 (SSAB, 2019), where arc efficiency (η) was considered to be 0.7 (Hackenhaar, Mazzaferro, Gonzalez, & Machado, 2016). The welding was performed using direct current electrode negative (DCEN) and the shielding gas adopted was pure argon. The welding parameters were selected through several experiments until the weld joint was acceptable (low distortions, full penetration, and absence of discontinuities). To minimize distortion the plates were held in position by clamping devices during the welding.

Table 1. Welding parameters employed in this study.

Welding parameters			
Current ($\boldsymbol{U}$)	180 A	Electrode diameter (EWTh2)	2.4 mm
Voltage ($\boldsymbol{I}$)	11 V	Electrode tip angle	60°
Welding speed ($\boldsymbol{v}$)	20 mm s^{-1}	Welding energy (E)	69.30 J mm^{-1}
Distance electrode tip-work	3 mm	Argon flow	15 l min^{-1}

$$E = \eta \cdot \frac{U \cdot I}{v} \qquad (2)$$

A schematic drawing of the welded joint is presented in Figure 2. The welding was performed in the same direction of rolling. The normal, transversal and longitudinal directions of the rolling process are referred as ND, TD and LD, respectively. Macro and micro observations, sliding wear tests and microhardness measures were executed in samples prepared with standard metallographic practice, followed by etching in 10% Nital.

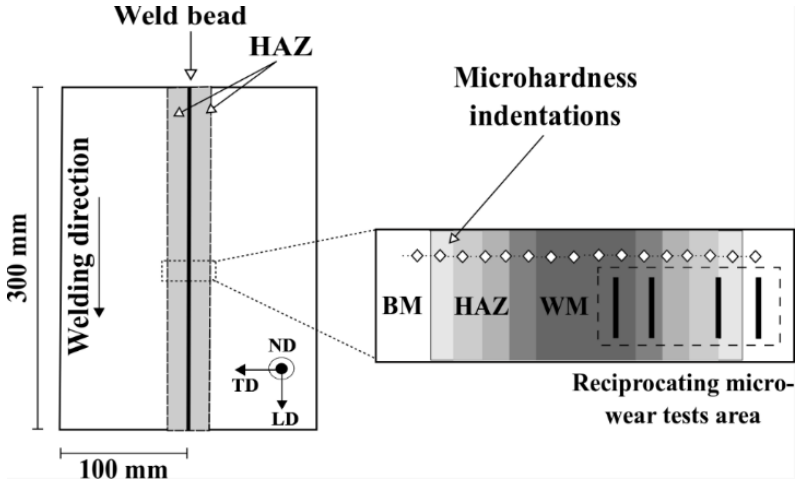

Figure 1. Schematic drawing (not to scale) of the welded joint and reciprocating micro-wear tests area.

The microhardness measurements were carried out on ND plane (normal direction of rolling process) using a semi-automatic microhardness tester. These tests were performed at a load of 300g during 10s using a Vickers pyramid micro indenter. Microhardness profiles were determined by taking microhardness readings along lines perpendicular to the welded joint as shown in Figure 2. These profiles were used to identify the gradient of microstructures (HAZ sub-zones) and the locations where reciprocating sliding micro-wear tests were later performed. Microhardness measures were carried out as per ASTM E384-17. The microhardness value obtained for as-received condition was 499 ± 6 HV.

In order to evaluate the influence of the weld resulting microstructure and HAZ softening on wear resistance, reciprocating sliding micro-wear tests were performed at BM, WM, CG-HAZ and LHR-HAZ sub-zone using a tribometer developed at Welding & Related Techniques Laboratory of Federal University of Rio Grande do Sul. The reciprocating micro-wear tests were performed on ND plane using Al_2O_3 balls with 4.762 mm diameter in ball-on-flat configuration. The tribometer device was able to

record the coefficient of friction (CoF) continuously during micro-wear tests. CoF medium values reported in this work were calculated excluding first 15 minutes data, to provide that Al_2O_3 balls have settled on the worn surface. All tests were carried out in dry condition under 10 N load. The linear sliding speed was 4 mm/s and the reciprocating stroke was set as 2 mm, with oscillation frequency of 1 Hz. The reciprocating micro-wear tests were performed during 2 h totaling a sliding distance of 28.8 m. The reciprocating micro-wear tests were repeated at least three times for each area.

After the wear tests, the worn tracks developed on the surface of the samples were analyzed by a 3D-profilometry, SEM and OM. In this study, the wear test results were quantified in terms of worn volume, which was calculated by integrating the area across the wear scar profile, and then multiplying the length of the tracks. Each worn trail had 10 cross-sectional profiles evaluated. ImageJ was used for computing the worn volumes of Al_2O_3 measuring the area of worn surfaces on OM images as per ASTM G133-05.

Results and discussion

Welded joint: microscopy and hardness

The macrostructures of welded joint on TD and ND (polished and etched) planes are presented in Figure 3. The samples were successfully autogenous welded in full penetration. Some distortions along the weld bead were observed. No weld defects such as pores and cracks were found.

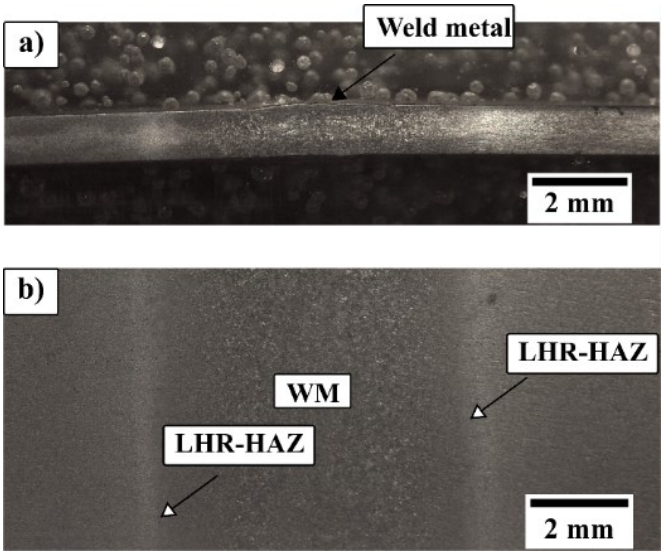

Figure 3. Macrostructure of the welded joint on: a) transversal direction (TD) and; b) normal direction (ND) of rolling process. On ND plane two different regions of the weld-joint, weld metal (WM) and the lowest hardness region of the heat affected zone (LHR-HAZ) is shown.

The microhardness profile across the weld-joint is shown in Figure 4. The highest microhardness average value was obtained on BM (499 ± 6 HV) followed by WM (452 ± 10 HV) and CG-HAZ (419 ± 9 HV). At LHR-HAZ microhardness value was 253 ± 6 HV, where hardness reduction reached a range of 50% compared to BM. HAZ extension was approximately 11 mm. BM structure is fully martensitic which is a thermally unstable phase, because of that it will tend to transform during welding, resulting in microstructural changes and softening of the local microstructure along the welded joint.

The microstructure of WM is composed by martensite - in this region the initial structure (BM) was melted and rapidly re-solidified resulting in a homogenous distribution of martensite presented in Figure 5. The microstructure of CG-HAZ was also martensite – this region is located immediately adjacent to the fusion boundary and was heated to temperatures high enough to enable the austenitic transformation, the generated austenite transforms to microstructures with less imperfect density and coarser grain size (Hochhauser, Ernst, Rauch, Vallant, & Enzinger, 2012). During subsequent cooling the coarse austenite is transformed into the martensitic structure presented in Figure 6. The presence of martensite at WM and CG-HAZ is controlled by cooling rate, which decreases while moving from the weld bead center. The martensite structure in these regions are coarser than BM, the hardness reduction on WM and CG-HAZ were respectively 10 and 16%.

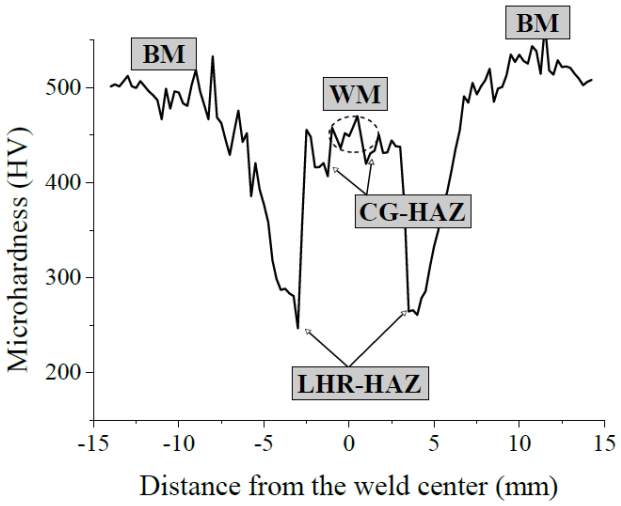

Figure 4. Microhardness profile across the welded joint.

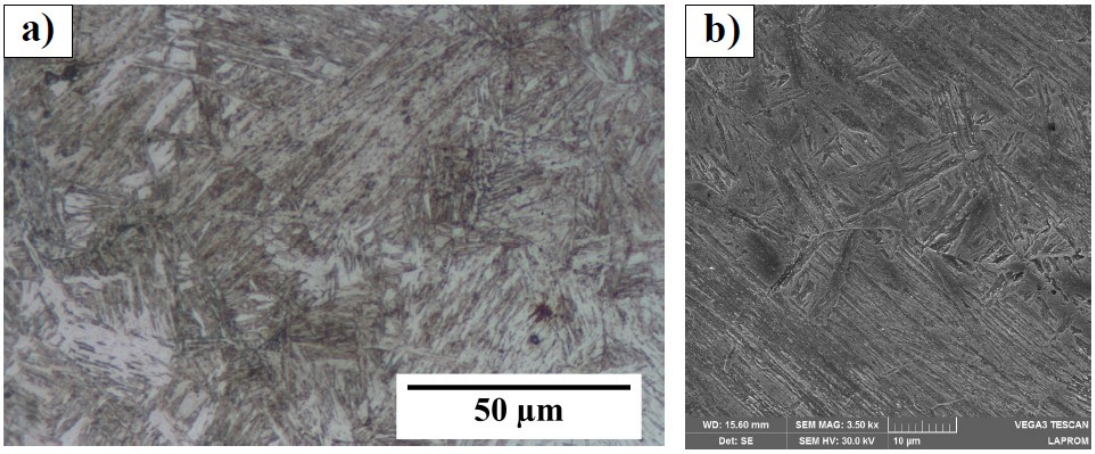

Figure 5. Martensitic structure of the weld metal: a) optic microscopy (OM); and b) scanning electron microscopy (SEM).

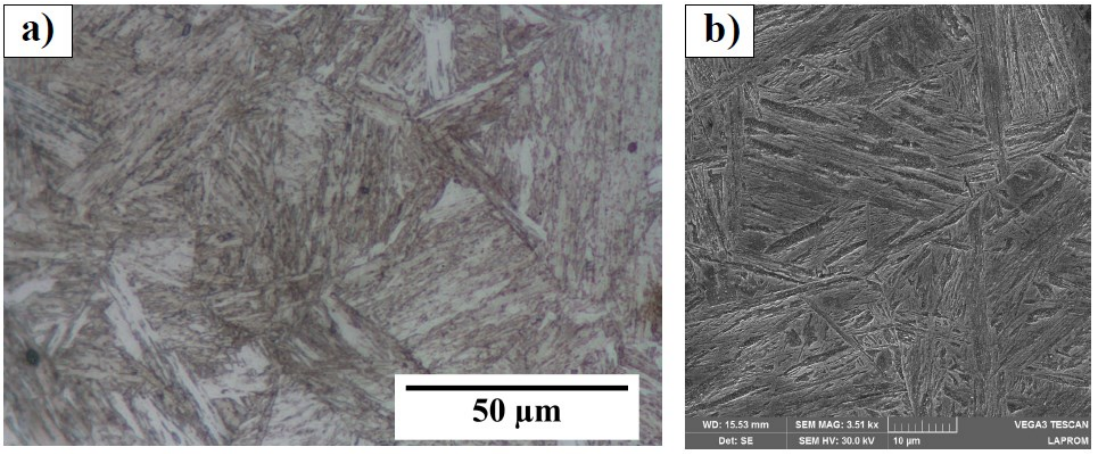

Figure 6. Martensitic structure of the coarse-grained heat affected zone: a) optic microscopy (OM); and b) scanning electron

At LHR-HAZ the microstructure was prevailingly over tempered martensite (M) with a mixture of ferrite (F) and carbides (C), as presented in Figure 7. These microstructure features indicate that heating during welding provoked the intensification of carbides precipitation from the initial tempered martensite (BM). Still during heating these carbides coalesced and some of them were dissolved to originate small austenite grains, which during cooling decompose to ferrite (Unfried, Garzon, & Giraldo, 2009). Softening phenomena was observed in this region, which is located at IC-HAZ/SC-HAZ interface. This result is in agreement with other authors who showed in their works that HAZ softening in martensitic steel weld-joints was predominantly controlled by over tempering of martensite

and formation of fresh ferrite in the SC-HAZ and in IC-HAZ (Biro et al., 2014; Frydman, Konat, & Pękalski, 2008; Guzman-Aguilera et al., 2018; Krishnan et al., 2006; Lu et al., 2018; Pandey et al., 2019; Pouranvari et al., 2018; Wang et al., 2016).

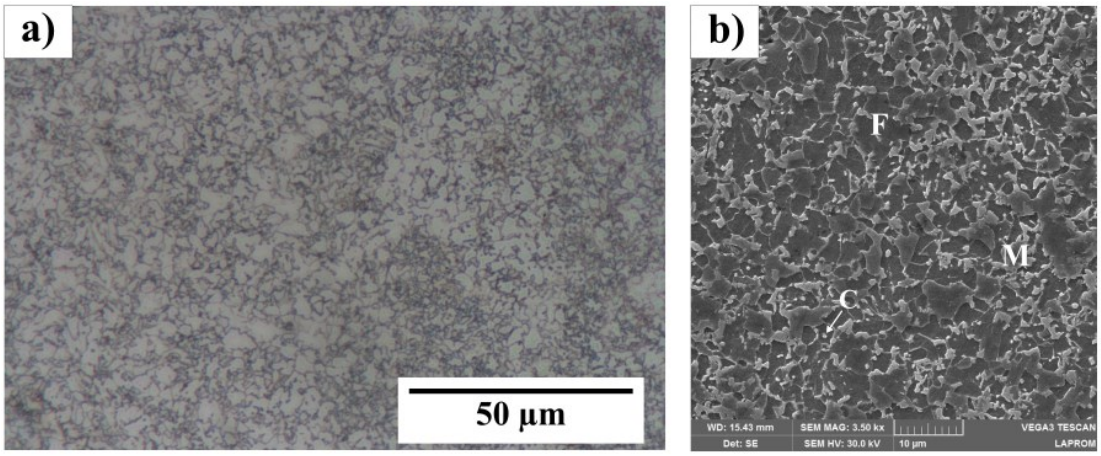

Figure 7. Microstructure of the lowest hardness region of the heat affected zone with over-tempered martensite (M), carbides (C) and ferrite (F): a) optic microscopy (OM); and b) scanning electron microscopy (SEM).

Sliding micro-wear behaviour

Table 3 presents the worn volumes of trails (w_t) and Al_2O_3 balls (w_b) used in the respective reciprocating sliding micro-wear tests. For the welded joint, the lowest worn volume average value was found in WM, followed by BM and CG-HAZ. The highest worn volume among the welded regions was obtained in LHR-HAZ. At this region the wear mechanisms related to plastic deformation were facilitated, which increased material removal by adhesion.

Table 2. Worn volumes (x10^{-5} mm^3) of trails (w_t) and Al_2O_3 balls (w_b).

	w_t	w_b
WM	2.78 ± 0.33	4.02 ± 0.19
CG-HAZ	3.41 ± 0.13	4.18 ± 0.21
LHR-HAZ	9.24 ± 0.36	3.95 ± 0.14
BM	3.36 ± 0.63	4.07 ± 0.07

The WM worn trail surface is presented in Figure 8 and 9a. In this region the material loss is mostly due to abrasion. Some detachment sites were also identified in Figure 8, however, adhesion occurred in much less pronounced form. The worn surface of the Al_2O_3 balls used in the reciprocating micro-wear tests in WM is presented in Figure 9b, the balls presented a circular smooth worn surface delimited by debris. The cross-sectional profile of the worn trail indicates that most of the abrasion grooves was shallow and their density per unit area was low, as showed in Figure 9c. According to Bhushan (2000) and Stachowiak and Batchelor (1993), these features suggest that most abrasive wear occurs on micro-ploughing form. Compared to micro-cutting, micro-ploughing leads to discreet wear damage, which resulted in the lowest worn volume. In this case, most of material removed from the grooves was only shifted to its borders, and then plastically deformed and dislocated.

The CG-HAZ worn trail surface is presented in Figure 10 and 11a. On this region material removal was due mostly to abrasion and adhesion. Similarly, to WM, the Al_2O_3 balls used in the reciprocating micro-wear tests, also presented a circular smooth worn surface delimited by debris, as showed in Figure 11b. The cross-sectional profile of the worn surface presented in Figure 11c shows shallow abrasion grooves, suggesting that abrasive wear occurred on micro-ploughing form.

The worn surfaces of the trails at LHR-HAZ are presented in Figure 12 and 13a. On this region the main wear mechanisms were adhesion and abrasion on micro-ploughing form, as showed in the cross-sectional profile of the worn surface presented in Figure 13c. The Al_2O_3 balls used as counter body presented a smooth circular surface delimited by debris, as showed in Figure 13b. LHR-HAZ was severely softened during welding, the ferrite

transformation and the over-tempering process of the initial martensitic structure increased ductility, which facilitated the wear mechanisms associated to plastic deformation. LHR-HAZ suffered massive adhesive damage that resulted on a worn volume over 70% greater than WM.

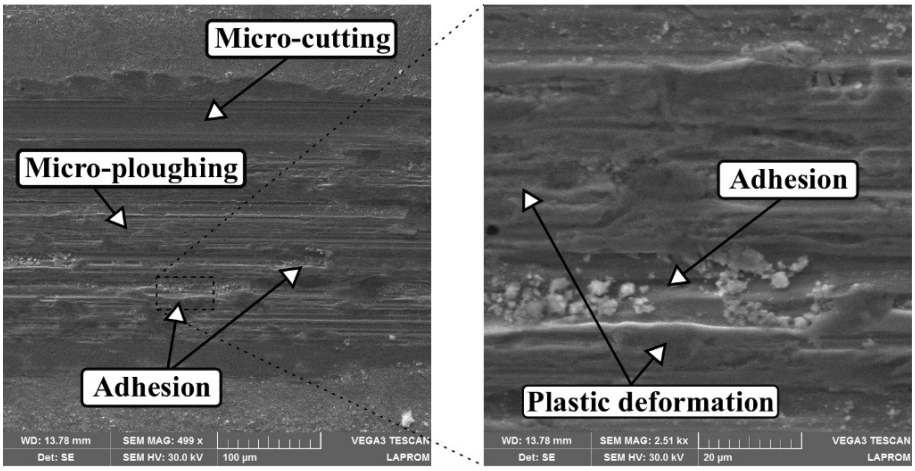

Figure 8. Worn trail surface of weld metal after reciprocating micro-wear test (SEM).

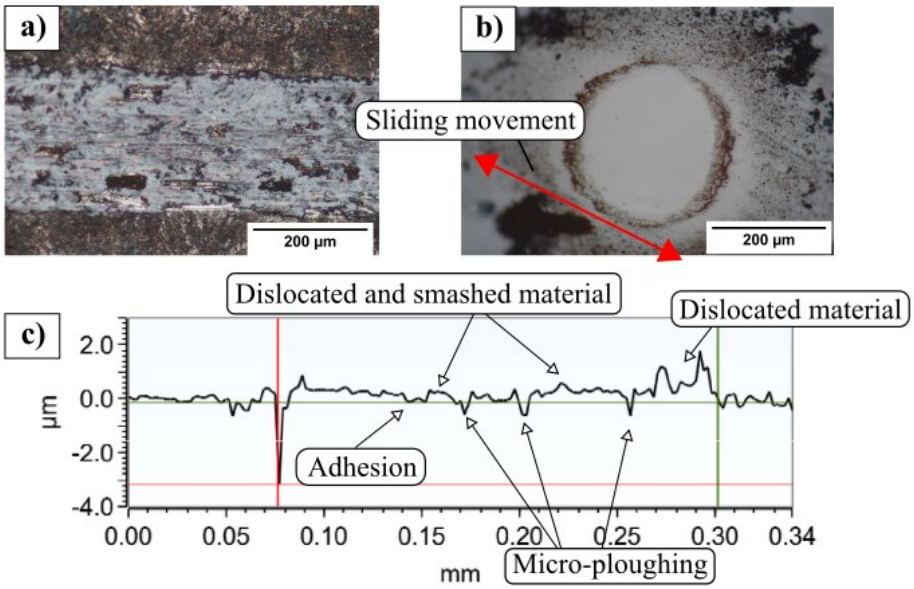

Figure 9.2 Weld metal: OM of a) worn trails and b) Al_2O_3 balls, and c) example of a cross-sectional profile of the worn trail obtained by surface profilometry, showing different micro-wear mechanisms.

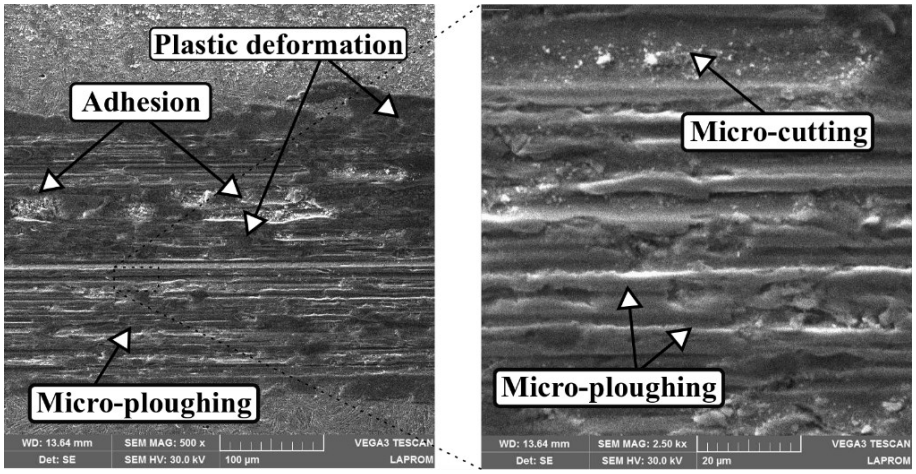

Figure 10. Worn trail surface of coarse-grained heat affected zone after reciprocating micro-wear test (SEM).

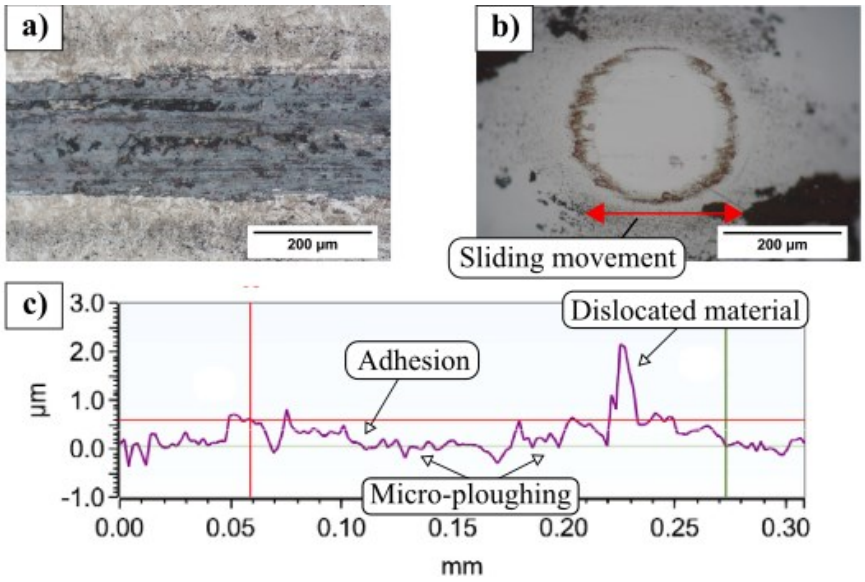

Figure 11. Coarse grained heat affected zone: OM of a) worn trails and b) Al_2O_3 balls; and c) example of a cross-sectional profile of the worn trail obtained by surface profilometry, showing different micro-wear mechanisms.

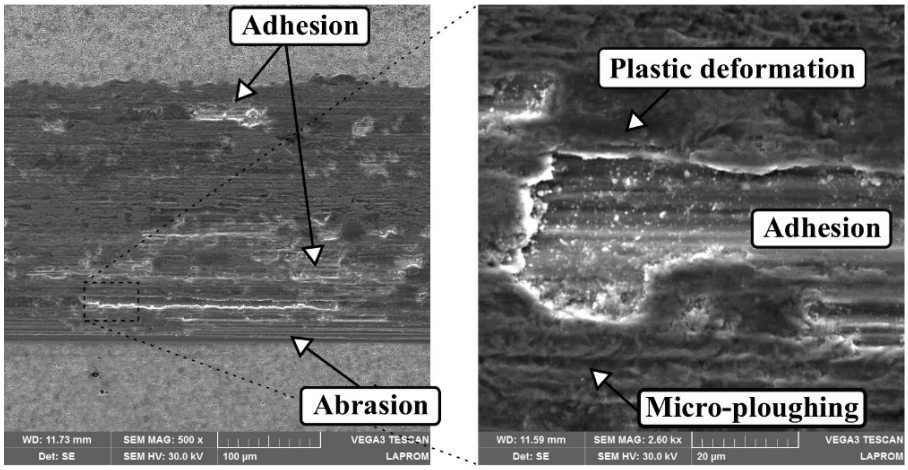

Figure 12. Worn trail surface of the lowest hardness region of heat affected zone after reciprocating micro-wear test (SEM).

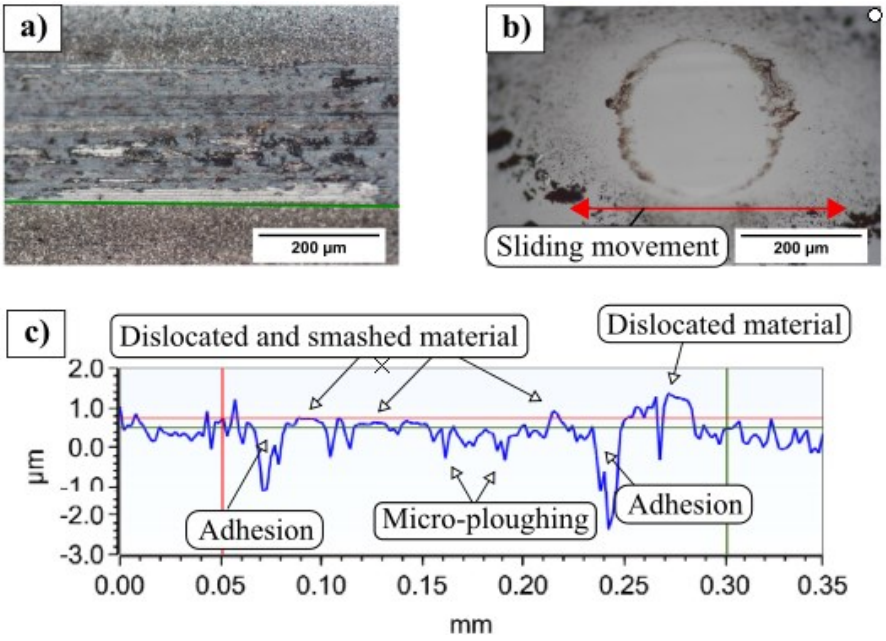

Figure 13. Lowest hardness region of heat affected zone: OM of a) worn trails and b) Al_2O_3 balls, and c) example of a cross-sectional profile of the worn trail obtained by surface profilometry, showing different micro-wear mechanisms.

For the BM most of the specimens presented a slight amount of material loss ($w_t = 3.36\,x\,10^{-5} mm^3$) caused by micro-ploughing. The abrasion grooves were shallow and no evidence of wear damage by three-body abrasion was found, as showed in Figures 14 and 15a and c. Figure 15b shows the Al_2O_3 balls surface. For these tests, the balls presented a smooth worn surface where no traces of debris were found.

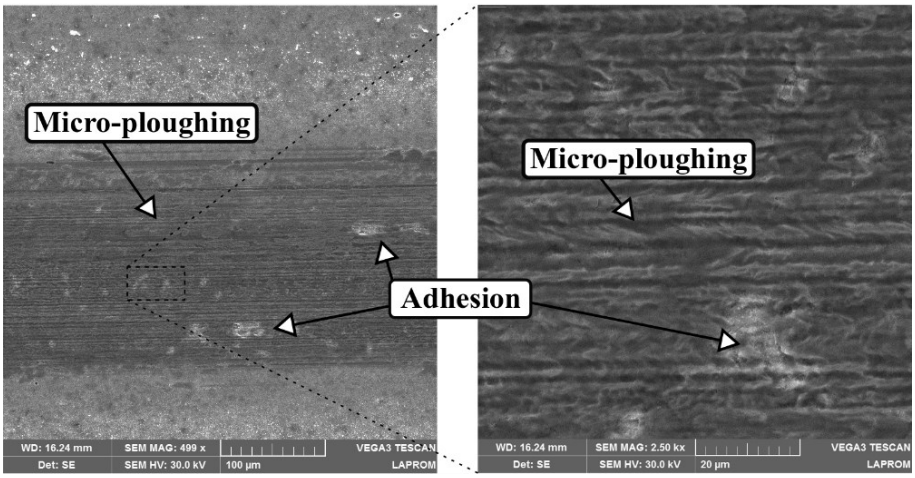

Figure 14. Slightly worn trail surface of base metal after reciprocating micro-wear test (SEM).

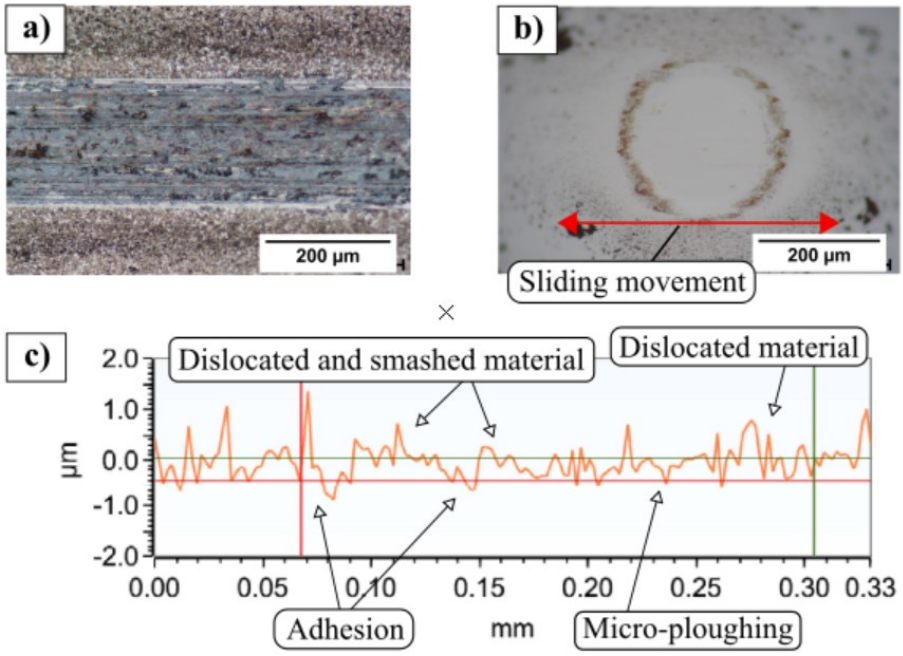

Figure 15. Base metal with slight and uniform abrasive wear damage: OM of a) worn trails and b) Al_2O_3 balls, and c) example of a cross-sectional profile of the worn trail obtained by surface profilometry, showing different micro-wear mechanisms.

Even though BM presents high hardness, some samples presented regions were massive wear damage by abrasion occurred. Compared to the BM samples where abrasion damage is uniform and slight along the full length of the trails, the material loss is up to 9 times greater. Figures 16 and 17a present the regions where severe wear damage occurred. According to other works (Guzman-Aguilera et al., 2018; Saroj, Sahoo, Tijo, Kumar, & Masanta, 2017), these deep grooves (Figure 17a) are usually caused by the presence of hard particles (debris) that slide over the surface causing the removal of material along its path.

Debris increase abrasive wear resulting in deeper grooves and massive wear damage. Besides that, according to Kirk, Shipway, Sun and Bennett (2019) debris can also adhere to the surfaces contributing to adhesive wear, which could explain the large detachments sites in Figure 16. The worn surface of the Al_2O_3 balls presented in Figure 17b also shows evidences of debris action. In fact, these features indicate

that abrasion occurred on three-body mode, which causes greater material loss (Bhushan, 2000; Stachowiak & Batchelor, 1993).

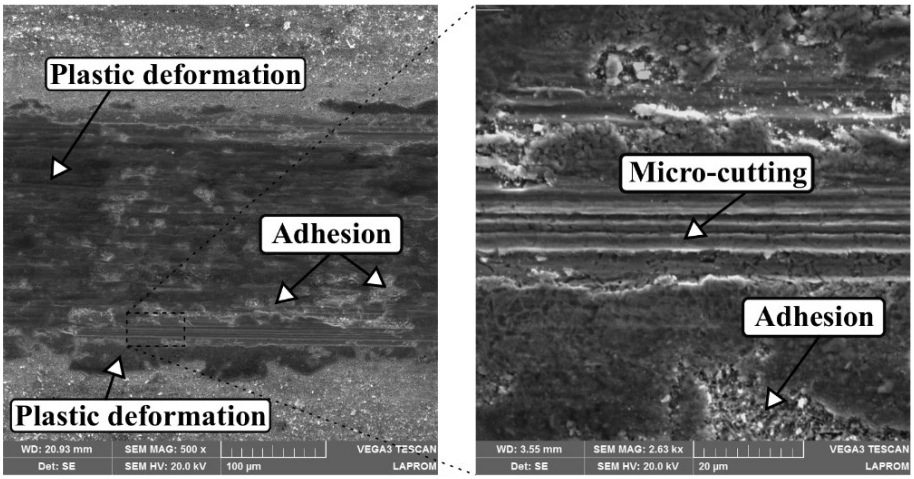

Figure 16. Severely worn trail surface of base metal after reciprocating micro-wear test (SEM).

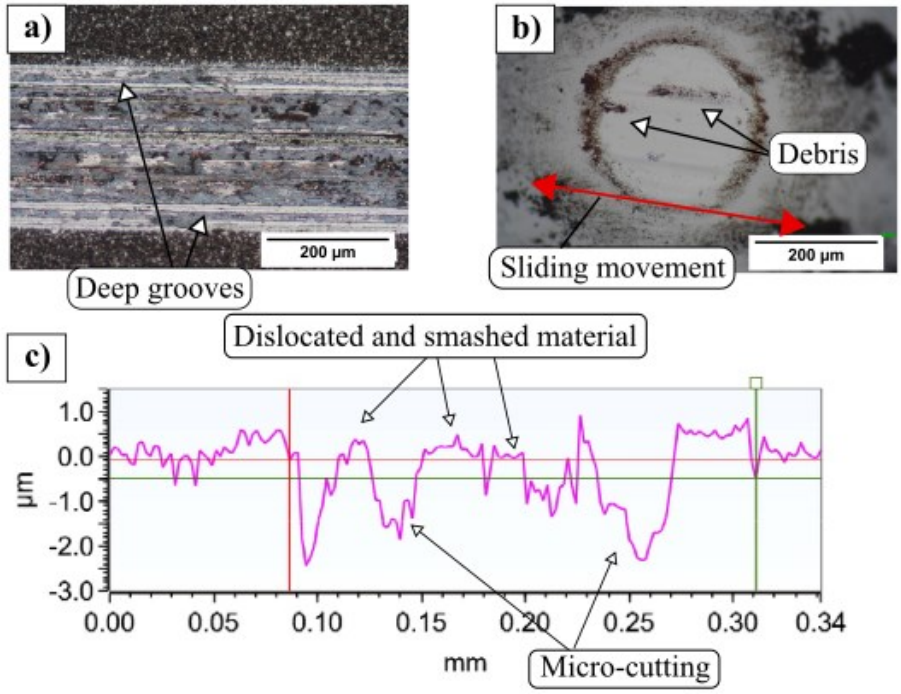

Figure 17. Base metal with massive micro-cutting wear damage: OM of a) worn trails and b) Al_2O_3 balls, and c) example of a cross-sectional profile of the worn trail obtained by surface profilometry, showing different micro-wear mechanisms.

During reciprocating sliding micro-wear tests debris are formed with different sizes depending on the tribological conditions (Bhushan, 2000; Hokkirigawa, & Kato, 1988). It is likely that during reciprocating sliding some debris particles were trapped on the contact surface and hardened, increasing debris abrasiveness and promoting massive wear damage on micro-cutting form along contact surface. Al_2O_3 balls and steel possess poor chemical affinity; because of that balls wear is due only to abrasion. However, debris accumulation on the worn surface can increase chemical affinity with worn trails surface, thus increasing adhesive wear on trails. Note that debris may increase materials loss due to adhesion and abrasion simultaneously.

Hardness is often used to predict the wear resistance of materials exposed to abrasion (Frydman et al., 2008; Mindivan, 2013; Sundström, Rendón, & Olsson, 2001) and according to Bhushan (2000) abrasive wear is proportional to the sliding distance and inversely proportional to the hardness of the wearing material. However, many authors (Dalbert et al., 2019; Mindivan, 2013; Sundström et al., 2001; Trevisiol, Jourani, & Bouvier, 2017) state that hardness must be used with caution when it comes to predicting the

wear resistance of materials exposed to abrasion. Wear resistance of a material in a given tribosystem is strongly influenced by the system parameters as well as toughness, work-hardening ability, ductility, microstructure, wear mechanism, etc. (Atkins, 2009; Shah & Bakshi, 2018; Sundström et al., 2001; Trevisiol et al., 2017).

In this study, wear resistance seems to be controlled by hardness. BM, WM and CG-HAZ presented a similar martensitic structure that was responsible for the discreet wear damage of trails. At LHR-HAZ the microstructure was severely softened leading to a greater material loss by plastic deformation related mechanisms.

Coefficient of friction

Coefficients of friction (CoF) values of the BM, WM, CG-HAZ and LHR-HAZ are presented in Table 4. Figure 18 shows the relationship between CoF values of the regions of interest on the welded joint and BM. CG-HAZ had the lowest CoF average value, followed by BM. WM and LHR-HAZ presented quite similar CoF, in the range of 0.43 - 0.44. CoF is minimized by region with the highest volume fraction of martensite (CG-HAZ) where less plastic deformation occurred. The highest CoF was reached for the softest sample.

It is shown in Figure 18 that the initial stage of the friction is unstable, and the CoF value continuously increases during this stage with fluctuations. According to Li, Deng, Huang, Ji and Wang (2019), these fluctuations on CoF values at the beginning of sliding wear tests is due to the fact that the upper and lower friction pairs are uneven surfaces in the running-in process. The interaction between the friction pairs causes the settlement of the Al_2O_3 balls on metal surface, which increases CoF. As the number of reciprocating slides increases, the CoF values begin to stabilize.

Table 4. Coefficient of friction of the welded joint regions.

	CoF
BM	0.40 ± 0.01
WM	0.43 ± 0.01
CG-HAZ	0.37 ± 0.02
LHR-HAZ	0.44 ± 0.02

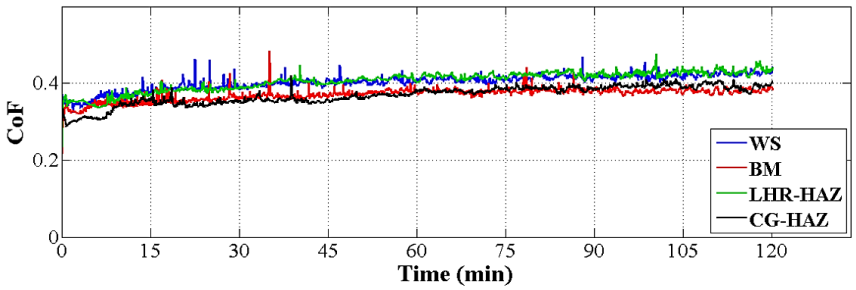

Figure 18. Examples of evolution of the coefficient of friction during reciprocating micro-wear tests.

Conclusion

In this study, the influence of welding on the reciprocating sliding wear under dry condition of quenched and tempered carbon martensitic steel was investigated. The main results are summarized as follow:

- Microstructure features, debris action, hardness and toughness seem to have an important role on micro-wear mechanisms which in turn are key factors controlling material removal;
- For the welded joint, the lowest worn volume average value was found in WM, followed by CG-HAZ, and both presented a similar martensitic structure after welding. For these regions, most material removal was due mostly by micro-ploughing;
- In a very narrow area at IC-HAZ/SC-HAZ interface, HAZ softening was observed, caused by a degradation of the initial martensitic structure after welding process. The microhardness reduction reached 50% in comparison with BM. This region in the welded joint showed the highest volume loss during sliding wear tests;

• Related to BM, debris had a key role on wear resistance. In some BM samples, debris acted as a third-body and promoted material loss by micro-cutting mechanism, which increased material loss in some regions. For those tests where only micro-ploughing was observed, worn volume value was smaller because most of the deformed material was smashed back into worn trails surface, decreasing material removal.

Acknowledgements

The authors gratefully acknowledge financial support from Coordination for the improvement of Higher Education Personnel (CAPES). The authors also gratefully acknowledge SSAB for providing the base material and Mineral Processing Laboratory and Multiuser Surface Analysis Laboratory for the equipment used in this study.

References

Atkins, T. (2009). Toughness and processes of material removal. *Wear*, *267*(11), 1764-1771. doi: 10.1016/j.wear.2009.04.010

Bhushan, B. (Ed.). (2000). *Modern Tribology Handbook*. Boca Raton, FL: CRC Press.

Białobrzeska, B., Dziurka R., Żak, A., & Bała, P. (2018). The influence of austenitization temperature on phase transformations of supercooled austenite in low-alloy steels with high resistance to abrasion wear. *Archives of Civil and Mechanical Engineering*, *18*(2), 413- 429. doi: 10.1016/j.acme.2017.09

Białobrzeska, B., & Kostencki P. (2015). Abrasive wear characteristics of selected low-alloy boron steels as measured in both field experiments and laboratory tests. *Wear*, *328-329*, 149-159. doi: 10.1016/j.wear.2015.02.003

Biro E., McDermid, J. R., Vignier S., & Zhou, Y. N. (2014). Decoupling of the softening processes during rapid tempering of a martensitic steel. *Materials Science and Engineering: A*, *615*, 395-404. doi: 10.1016/j.msea.2014.07.102

Dalbert, V., Mary, N., Normand, B., Verdu, C., Douillard, T., & Saedlou, S. (2019). The effects of microstructures and repassivation kinetics on the tribocorrosion resistance of ferrite and ferrite-martensite stainless steels. *Wear*, *420-421*, 245-256. doi: 10.1016/j.wear.2018.10.023

Frydman, S., Konat, Ł., & Pękalski, G. (2008). Structure and hardness changes in welded joints of Hardox steels. *Archives of Civil and Mechanical Engineering*, *8*(4), 15-27. doi: 10.1016/S1644-9665(12)60118-6

Guzman-Aguilera, J. J., Martinez-Gonzalez, C. J., Baltazar-Hernandez, V. H., Basak, S., Panda, S. K., Razmpoosh, M. H., ... Zhou, Y. (2018). Influence of SC-HAZ microstructure on the mechanical behavior of Si-TRIP steel welds. *Materials Science and Engineering: A*, *718*, 216- 227. doi: 10.1016/j.msea.2018.01.108

Hacisalihoğlu, I., Yildiz, F., & Çelik, A. (2018). Tribocorrosion behavior of plasma nitrided Hardox steels in NaCl solution. *Tribology International*, *120*, 434-445. doi: 10.1016/j.triboint.2018.01.023

Hackenhaar, W., Mazzaferro, J. A. E., Gonzalez, A. R., & Machado, I. G. (2016). Influência da vazão e geometria da região de entrada sobre a eficiência térmica medida por um calorímetro de fluxo contínuo de água. *Soldagem & Inspeção*, *21*(3), 269-281. doi: 10.1590/0104-9224/SI2103.03

Hernandez, S., Hardell, J., Winkelmann, H., Ripoll, M. R., & Prakash, B. (2015). Influence of temperature on abrasive wear of boron steel and hot forming tool steels. *Wear*, *338-339*, 27-35. doi: 10.1016/j.wear.2015.05.010

Hochhauser, F., Ernst, W., Rauch, R., Vallant, R., & Enzinger, N. (2012). Influence of the soft zone on the strength of welded modern HSLA steels. *Welding in the World*, *56*, 77-85. doi: 10.1007/BF03321352

Hokkirigawa, K., & Kato, K. (1988). An experimental and theoretical investigation of ploughing, cutting and wedge formation during abrasive wear. *Tribology International*, *21*(1), 51-57. doi: 10.1016/0301-679X(88)90128-4

Ilanaganar, E., & Anbuselvan, S. (2018). Wear mechanisms of AZ31B magnesium alloy during dry sliding condition. *Materials Today: Proceedings*, *5*(1, Pt. 1), 628-635. doi: 10.1016/j.matpr.2017.11.126

Kirk, A., Shipway, P., Sun, W., & Bennett, C. (2019). Debris development in fretting contacts: debris particles and debris beds. *Tribology International*, *149 (105592)*, 1-9. doi: 10.1016/j.triboint.2019.01.051

Krishnan, S. N., Toppo, V., Basak, A., & Ray, K. K. (2006). Wear behaviour of a steel weld-joint. *Wear*, *260*(11-12), 1285-1294. doi: 10.1016/j.wear.2005.08.007

Li, C., Deng, X., Huang, L., Jia, Y., & Wang, Z. (2019). Effect of temperature on microstructure, properties and sliding wear behavior of low alloy wear-resistant martensitic steel. *Wear*, *442-443 (203125)*, 1-8. doi: 10.1016/j.wear.2019.203125

Lu, Y., Peer, A., Abke, T., Kimchi, M., Zhang, W. (2018). Subcritical heat affected zone softening in hot-stamped boron steel during resistance spot welding. *Materials & Design*, *155*, 170-184. doi: 10.1016/j.matdes.2018.05.067

Mendez, P. F., Barnes, N., Bell, K., Borle, S. D., Gajapathi, S. S., Guest, S. D., Izadi, H., & Wood, G. (2014). Welding processes for wear resistant overlays. *Journal of Manufacturing Processes*, *16* (1), 4-25. doi: 10.1016/j.jmapro.2013.06.011

Mindivan, H. (2013). Effects of combined diffusion treatments on the wear behaviour of hardox 400 steel. *Procedia Engineering*, *68*, 710-715. doi: 10.1016/j.proeng.2013.12.243

Mishra, B., Kumbhar, K., Kumar, D., Sarkar, R., Kumar, K. S., & Srinivas, M. (2019). Effect of boron addition on microstructure and tensile properties of copper modified ultra high strength NiSiCrCoMo steel. *Materials Science and Engineering: A*, 744, 112-119. doi: 10.1016/j.msea.2018.12.003

Pandey, C., Mahapatra, M. M., Kumar, P., Daniel, F., & Adhithan B. (2019). Softening mechanism of P91 steel weldments using heat treatments. *Archives of Civil and Mechanical Engineering*, *19*(2), 297-310. doi: 10.1016/j.acme.2018.10.005

Pawlak, K., Białobrzeska, B., & Konat, Ł. (2016). The influence of austenitizing temperature on prior austenite grain size and resistance to abrasion wear of selected low-alloy boron steel. *Archives of Civil and Mechanical Engineering*, *16*(4), 913-926. doi: 10.1016/j.acme.2016.07.003

Pouranvari, M., Sobhani S., & Goodarzi F. (2018). Resistance spot welding of MS1200 martensitic advanced high strength steel: Microstructure-properties relationship. *Journal of Manufacturing Processes*, *31*, 867-874. doi: 10.1016/j.jmapro.2018.01.009

Pujari, K. S., Patil, D. V., & Mewundi, G. (2018). Selection of GTAW process parameter and optimizing the weld pool geometry for AA 7075-T6 aluminum alloy. *Materials Today: Proceedings*, *5*(11, Pt. 3), 25045-25055. doi: 10.1016/j.matpr.2018.10.305

Saroj, S., Sahoo, C. K., Tijo, D., Kumar, K., & Masanta, M. (2017). Sliding abrasive wear characteristic of TIG cladded TiC reinforced inconel825 composite coating. *International Journal of Refractory Metals and Hard Materials*, *69*, 119-130. doi: 10.1016/j.ijrmhm.2017.08.005

Shah, M., & Bakshi, S. D. (2018). Three-body abrasive wear of carbide-free bainite, martensite and bainite-martensite structure of similar hardness. *Wear*, *402-403*, 207-215. doi: 10.1016/j.wear.2018.02.020

SSAB. (2019). *Hardox Wear Plate. Data sheet 168uk Hardox 450*. Retrieved from https://bitlybr.com/grFPzocZ

Stachowiak, G. W., & Batchelor, A. W. (1993). 11 Abrasive, Erosive and Cavitation Wear. *Tribology Series*, 24, 557-612. doi: 10.1016/S0167-8922(08)70585-6

Sundström, A., Rendón, J., & Olsson M. (2001). Wear behaviour of some low alloyed steels under combined impact/abrasion contact conditions. *Wear*, *250*(1), 744-754. doi: 10.1016/S0043-1648(01)00712-8

Trevisiol, C., Jourani, A., & Bouvier, S. (2017). Effect of hardness, microstructure, normal load and abrasive size on friction and on wear behaviour of 35NCD16 steel. *Wear*, *388-389*, 101-111. doi: 10.1016/j.wear.2017.05.008

Unfried, J. S., Garzon, C. M., & Giraldo, J. E. (2009). Numerical and experimental analysis of microstructure evolution during arc welding in armor plate steels. *Journal of Materials Processing Technology*, *209*(4), 1688-1700. doi: 10.1016/j.jmatprotec.2008.04.025

Vasantharaja, P., Vasudevan, M., & Parameswaran, P. (2019). Effect of welding techniques on the microstructure and mechanical properties of reduced activation ferritic-martensitic (RAFM) steel weld joints. *Fusion Engineering and Design*, 148, 1-10. doi: 10.1016/j.fusengdes.2019.111289.

Wang, J., Yang, L., Sun, M., Liu, T., & Li, H. (2016). A study of the softening mechanisms of laser-welded DP1000 steel butt joints. *Materials & Design*, *97*, 118-125. doi: 10.1016/j.matdes.2016.02.071

Xu, X., Zwaag, S., & Xu, W. (2016). The scratch and abrasive wear behaviour of a tempered martensitic construction steel and its dual phase variants. *Wear*, *358-359*, 80-88. doi: 10.1016/j.wear.2016.04.005